

Impacts of Diurnal Variation of Mountain-plain Solenoid Circulations on Precipitation and Vortices East of the Tibetan Plateau during the Mei-yu Season

ZHANG Yuanchun^{1,2}, SUN Jianhua^{*1,3}, and FU Shenming¹

¹*Institute of Atmospheric Physics, Chinese Academy of Sciences, Beijing 100029*

²*Graduate University of the Chinese Academy of Sciences, Beijing 100049*

³*State Key Laboratory of Severe Weather, Chinese Academy of Meteorological Sciences, Beijing 100084*

(Received 6 August 2012; revised 14 March 2013; accepted 15 March 2013)

ABSTRACT

Diurnal variations of two mountain-plain solenoid (MPS) circulations associated with “first-step” terrain [Tibetan Plateau (TP)] and “second-step” terrain (high mountains between the TP and “east plains”) in China and their influence on the southwest vortex (SWV) and the mei-yu front vortex (MYFV) were investigated via a semi-idealized mesoscale numerical model [Weather Research and Forecasting (WRF)] simulation integrated with ten-day average fields (mei-yu period of 1–10 July 2007). The simulations successfully reproduced two MPS circulations related to first- and second-step terrain, diurnal variations from the eastern edge of the TP to the Yangtze River–Huaihe River valleys (YHRV), and two precipitation maximum centers related to the SWV, MYFV. Analyses of the averaged final seven-day simulation showed the different diurnal peaks of precipitation at different regions: from the afternoon to early evening at the eastern edge of the TP; in the early evening to the next early morning in the Sichuan Basin (SCB); and in the late evening to the next early morning over the mei-yu front (MYF). Analyses of individual two-day cases confirmed that the upward branches of the nighttime MPS circulations enhanced the precipitation over the SWV and the MYFV and revealed that the eastward extension of the SWV and its convection were conducive to triggering the MYFVs. The eastward propagation of a rainfall streak from the eastern edge of the TP to the eastern coastal region was primarily due to a series of convective activities of several systems from west to east, including the MPS between the TP and SCB, the SWV, the MPS between second-step terrain and the east plains, and the MYFV.

Key words: mountain-plain solenoid (MPS), diurnal variation, mei-yu front

Citation: Zhang, Y. C., J. H. Sun, and S. M. Fu, 2014: Impacts of diurnal variation of mountain-plain solenoid circulations on precipitation and vortices east of the Tibetan Plateau during the mei-yu season. *Adv. Atmos. Sci.*, **31**(1), 139–153, doi: 10.1007/s00376-013-2052-0.

1. Introduction

The Yangtze River–Huaihe River valleys (YHRV) suffers persistently from long-lasting rainstorms and severe flooding during the mei-yu season, which are caused by a quasi-stationary, 1000-km-long rain belt associated with the east–west oriented mei-yu front (MYF) from East Asia to the West Pacific during summer (Tao, 1980; Ding, 1993). Most Chinese meteorologists focus on the temporal and spatial characteristics of MYF vortices (MYFV) along the Yangtze River–Huaihe River valleys, the Yangtze River valley or the Huaihe River valley over East China. Zhang et al. (2002) proposed a multi-scale schematic model for the control of MYF precipitation over East Asia, which included four simultaneously

active key factors: propagating short-wave troughs in the mid-latitude jet streams; short-term variations in the southwesterly monsoon flow; changes in the West Pacific Subtropical High; and the eastward-propagating convective systems from the Tibetan Plateau (TP). One of the four key factors is the meso- α -scale convective systems from the TP that propagate eastward to the YHRV and promote the formation and development of meso- α -scale convective systems along the MYF and subsequently enhance heavy rainstorms. Zhuo et al. (2002) revealed that convective systems originating over the TP merged with a local cloud cluster over the Yangtze River valley after being strengthened in the Sichuan Basin during a period of severe rainfall in July 1998. Yasunari and Miwa (2006) demonstrated that convection occurs east of the TP and that the convergence line occasionally extends to the eastern edge of the TP, which could trigger the southwest vortex (SWV). Subsequently, the SWV induces a strong low-

* Corresponding author: SUN Jianhua
E-mail: sjh@mail.iap.ac.cn

level jet (LLJ) with abundant moisture inflow to the east of the SWV, which facilitates further development of the vortex into a meso- α -scale cloud system embedded in the MYF over the Yangtze River valley.

However, the eastwardly propagating mechanisms of these systems from the TP and their detailed influences on MYF convective systems are not clearly understood. Because of the unique topographic distribution and monsoon climatology in East Asia, precipitation along the MYF exhibits complicated features determined by multi-scale atmospheric circulations (Zhang et al., 2004; Zhao et al., 2004), and possesses a certain diurnal variation (Akiyama, 1990; Ninomiya, 2000; Geng and Yamada, 2007; Yu et al., 2007). Previous studies have also shown that summertime convection in the Northern Hemisphere often develops over the high mountains in the local afternoon that subsequently propagates eastward across the leeside plains overnight due to forcing from diurnally varying heating (Wang et al., 2004, 2005; Trier et al., 2006, 2010; He and Zhang, 2010; Huang et al., 2010). In East Asia, the major terrain is the TP, which is often referred to as the “first-step” terrain in China. The “second-step” terrain in China usually refers to the high mountain ranges such as the Da Hinggan Mountains in Northeast China; the Yan-shan Mountains and the Taihangshan Mountains, the Loess Plateau and the Mongolian Plateau in North China; the Qin-ling Mountains in Central China; and the Yunnan-Guizhou Plateau in Southwest China. The “third-step” terrain includes the low-lying plains and hilly regions to the east of the second-step, and the high-mountain terrains (hereafter referred to as the “east plains”). The leeside nocturnal convection near the Sichuan Basin and surrounding areas in North China and in the YHRV have been studied previously (Wang et al., 2004, 2005; Yu et al., 2007).

Precipitation along the MYF in the YHRV with midnight to early-morning peaks is especially influenced by the mountain-plain solenoid (MPS) circulation that develops between the high mountains and the eastern low-lying basin or plains. Bao et al. (2011, hereafter referred to as BZ11) discussed the various diurnal variations and their synoptic circulations during the pre-meiyu period, during the meiyu period, and during the post-meiyu period, using analyses of National Oceanic and Atmospheric Administration (NOAA) Climate Prediction Center (CPC) morphing technique (CMORPH) rainfall data and an National Centers for Environmental Prediction Global Forecast System (Final) global gridded analysis (NCEP FNL) from 2003 to 2009. Even after this study, because of the low temporal and spatial resolution of the NCEP FNL, the influences of MPS circulation on the diurnal variation of precipitation along the MYF have not been described in detail. Sun and Zhang (2012, hereafter referred to as SZ12) indicated that an upward branch of the MPS circulation between the second-step terrain and the east plains increased the midnight to early-morning precipitation along the MYF east of 114°E. However, their study ignored the influence of the TP on its downstream area, focusing only on the area east of the TP. Previous studies have confirmed that the TP has significant effects on the synoptic

circulation of East Asia (Ye and Gao, 1979; Yang and Yang, 1987; Zhang et al., 1988). Therefore, based on these past studies, in this paper, we will use consecutive ten-day high-resolution numerical simulation results to study in detail the diurnal variations of MPS circulations between high mountains (first-step and second-step mountains) and their downstream basin or plains and their influences on the vortices and precipitation over the Sichuan Basin and the Huaihe River valley.

The primary goals of the current work are to reveal the diurnal variations of precipitation and vortices from the eastern edge of the TP to the eastern coastal region (including the Sichuan Basin and the MYF), to understand the impacts of diurnal variations and the interactions of the SWV and MYFV on the rain belt extending from the foot of the TP to the MYF, and to understand the possible impacts of a non-eastward-moving SWV on an MYFV. The second section introduces the studied event, its synoptic circulation pattern, and the experimental design. The third section compares the simulation to observations, and the fourth section analyzes the diurnal variations of simulated precipitation, SWV, MYFV and MPS circulations. The fifth section discusses diurnal variations of MPS circulations and their impacts on rainfall-producing systems, as well as the relationship between the SWV and MYFV during the simulated individual period of 4–6 July 2007. The final section contains concluding remarks.

2. The synoptic weather pattern of the studied event and the experimental design

The main mei-yu rain belt from 19 June to 26 July 2007 extended from the foothills of the TP to the east plains and resulted in severe flooding (Zhao et al., 2007; Fu et al., 2011). There were two rainfall centers with a maximum accumulated precipitation amount of greater than 400 mm during 1–10 July 2007, as derived from CMORPH data, which is a high-resolution, global precipitation dataset using the NOAA Climate Prediction Center’s morphing technique (Joyce et al., 2004) with a spatial resolution of 0.7277° (Fig. 1a). One rainfall center was located over the Huaihe River valley east of 110°E and extended from west to east, while the other covered the Sichuan Basin at approximately 105°E and extended from southwest to northeast. The synoptic weather pattern was highly conducive to the development of mesoscale convective systems along the MYF. At 500 hPa, there were two cut-off lows located over Baikal Lake and in Northeast China, while a synoptic ridge system dominated over Northwest China in the middle latitudes. The West Pacific Subtropical High dominated over southeastern China, with the 5860-m isohypse reaching as far west as 110°E in the low latitudes (Fig. 1a). The mid-latitude jet stream at 200 hPa persisted north of 35°N. At 850 hPa, there was an SWV over the Sichuan Basin and a shear line between the southwestlies and northeasterlies extending from the Sichuan Basin to the coastline (Fig. 1b). To the south of the shear line, there was a southwest LLJ on the northwest edge of the West

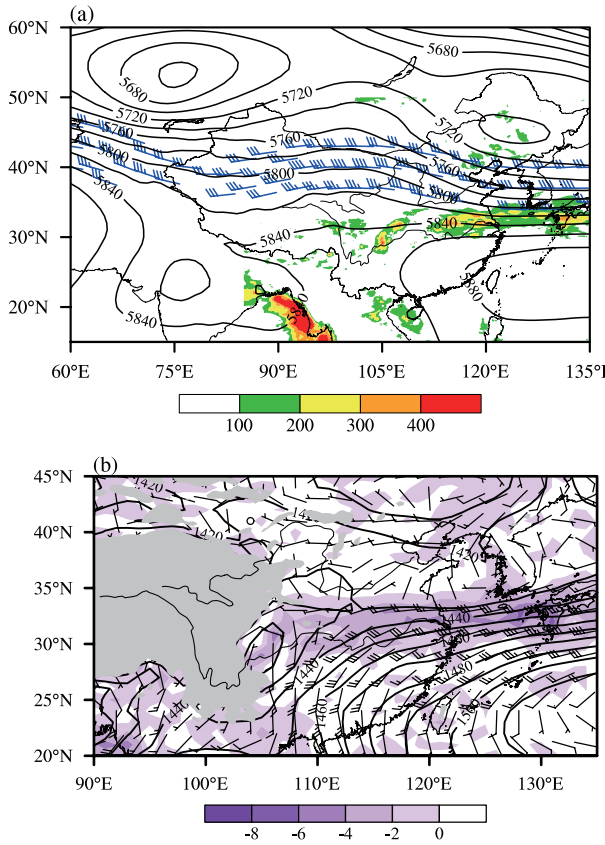


Fig. 1. Average fields from 0000 UTC 1 July to 0000 UTC 11 July 2007: (a) mean geopotential height (gpm) at 500 hPa and the upper-level jet greater than 30 m s^{-1} at 200 hPa (full bar: 10 m s^{-1}) and total precipitation (mm); (b) mean geopotential height (gpm), wind barb (full barb: 5 m s^{-1}) and divergence of the whole layer moisture flux (colored, $10^{-6} \text{ g cm}^{-2} \text{ s}^{-1}$) at 850 hPa.

Pacific Subtropical High, with a maximum wind speed that exceeded 12 m s^{-1} and that brought abundant warm and moist air to the precipitation areas. A strong convergence band of moisture flux existed from the Sichuan Basin to the Huaihe River valley in the lower troposphere, with maximum centers over the provinces of Henan, Anhui and Jiangsu.

The Weather Research and Forecasting (WRF) model, version 3.2 (Skamarock et al., 2005), was used for the current reported study. According to Trier et al. (2006, 2010), SZ12 studied the impacts of MPS circulation between the second-step terrain and east plains on the maximum precipitation center and its diurnal variation along the MYF through a semi-idealized simulation of the rainfall case. The result showed that the semi-idealized experiment successfully simulated the observed diurnal variation and eastward propagation of rainfall and mesoscale convective vortices (MCVs) along the MYF.

Based on previous studies, this study also simulated the heavy rainfall event of 1–10 July 2007 with the same initial and lateral boundary conditions as SZ12, but with the aim being to focus on the impacts of mesoscale systems upstream (including the eastern edge of the TP and Sichuan Basin) on

the diurnal variation of precipitation at the MYF and the triggering of mesoscale vortices along the MYF. The model was initialized with the mean of the FNL analysis at 0000 UTC averaged over the ten-day period of 1–10 July 2007 with lateral boundary conditions derived from the ten-day averages at 0000, 0600, 1200 and 1800 UTC, which cycle periodically with time. Such lateral boundary conditions only allowed the diurnal variation part of the transient processes to influence the simulation domain.

As the focus in this paper is the topographic impacts (including the eastern edge of the TP and second-step terrain), to avoid complications caused by the propagation of small-scale disturbances originating from the high latitudes and west of the TP, and from those disturbances entering the simulation domain, only one simulation domain was used. This simulation domain covered East Asia, including most parts of the TP and the monsoon regions south of the TP (20° – 36° N, 85° – 125° E), with $985(\text{lon}) \times 493(\text{lat})$ horizontal grid points and 4-km grid spacing (Fig. 2a). There were 28 vertical levels, with the top at 50 hPa. The model employed the Yonsei University (YSU) boundary layer scheme (Noh et al., 2001), the Noah land surface model (Chen and Dudhia, 2001), a long-wave and short-wave radiation parameterization (Dudhia, 1989), and a WSM 5-class microphysics parameterization (Hong et al., 2004; Hong and Lim, 2006). The initial fields showed that the West Pacific Subtropical High at 500 hPa covered southeastern China, and an SWV was located over the Sichuan Basin, with wind speed exceeding 10 m s^{-1} at 850 hPa (Fig. 2b). Consequently, the initial fields illustrated the typical synoptic circulation during the mei-yu period (Tao, 1980), and thus was highly conducive to simulating convection over the eastern edge of the TP and the precipitation over the Sichuan Basin and at the MYF, as well as simulating their diurnal variation and eastward propagation, as forced by the above initial and diurnal lateral boundary conditions.

3. Comparison of simulation and observation

To reduce the sensitivity to the initial conditions, only the final seven days of the ten-day simulation were examined in this paper. Although the accumulated precipitation in the simulation was stronger than that in observations during the final seven days (Fig. 3), two maximum precipitation centers, located over the Sichuan Basin and the Huaihe River valley, were similar to observations, except that the former was located slightly east of the observed location. The simulated precipitation intensity in SZ12 was also stronger in the simulation than the real case, which was caused by a more stable rain belt, forced by the diurnal lateral boundary conditions. However, the precipitation derived from CMORPH was relatively weak compared with that in observations from the surface station, especially at the maximum rainfall center (not shown), but the CMORPH data are for areas over both land and sea.

Figure 4 shows time-longitudinal cross sections of the diurnal hourly precipitation averaged from CMORPH data

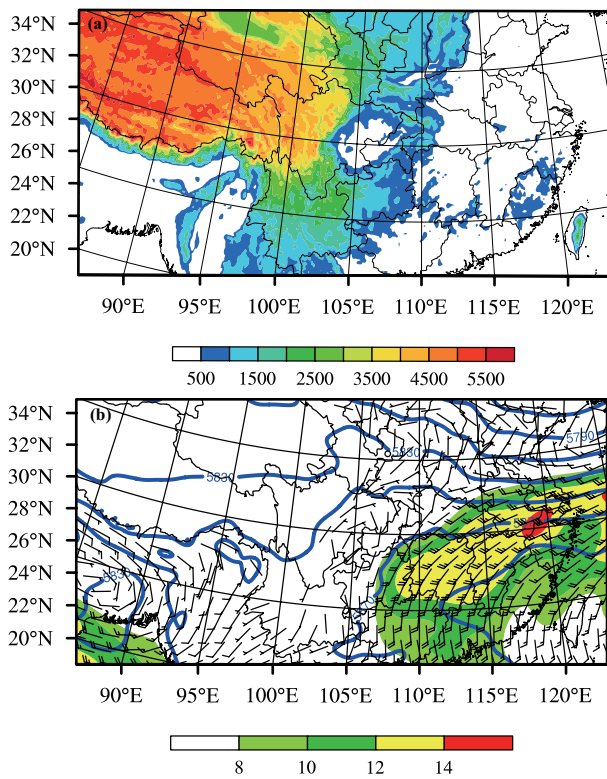


Fig. 2. (a) Configuration of the simulated domain and topography; (b) initial field of 500-hPa geopotential height (blue lines, gpm), 850-hPa wind vector (full barb: 5 m s^{-1}), and 850-hPa wind speed higher than 8 m s^{-1} (colored).

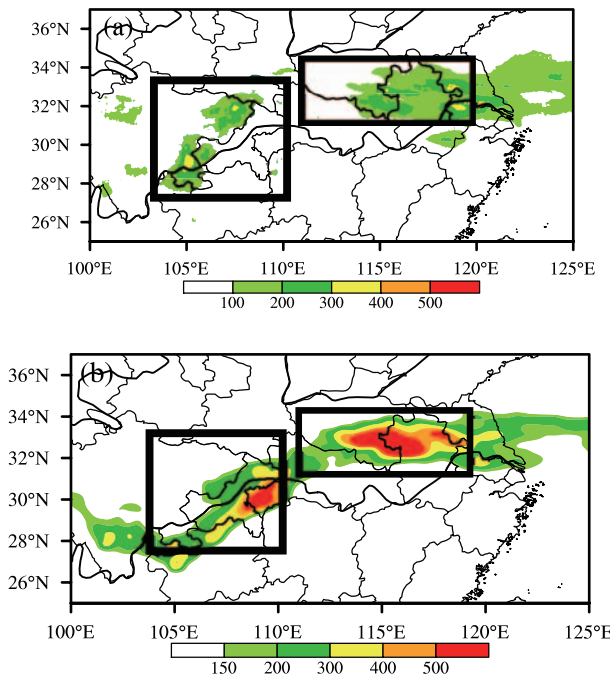


Fig. 3. Accumulated precipitation (units: mm) from 0000 UTC 4 July to 0000 UTC 11 July 2007: (a) CMORPH and (b) final seven-day simulation. The two rectangles indicate the southwest vortex (SWV) and mei-yu front vortex (MYFV).

during 4–10 July and the final seven-day simulation. The precipitation peak started at 0600 UTC at the eastern edge of the TP (100° – 103° E) and remained until 1800 UTC. This diurnal peak subsequently shifted downslope and reached the Sichuan Basin (at approximately 105° – 108° E) during the period 1000–2100 UTC, corresponding to the late evening and early morning rainfall maxima observed in this area (Yu et al., 2007; BZ11). The diurnal peak in the Sichuan Basin tended to weaken from the next morning to the afternoon. Despite the existence of thermal convection in the afternoon to early evening, the precipitation was relatively weak. Although the precipitation nearly persisted for the whole day along the MYF, the maximum rainfall appeared from evening to early morning (1200–0200 UTC), and the minimum occurred during the daytime (0300–1100 UTC), with a slight increase in the afternoon. Both the simulation and observations featured two maximum precipitation centers over the Sichuan Basin and the Yangtze River–Huaihe River valleys, as well as clearly propagating rainfall streaks from the eastern edge of the TP to the east plains. In spite of the precipitation centers at 108° E and 114° – 117° E being stronger in the simulation than in observations, the diurnal variation and eastward propagation features of both remained consistent with each other. According to the above analyses, it is reasonable to discuss the potential impacts of MPS circulations on the precipitation over the Sichuan Basin and along the MYF, as well as the interactions among rainfall-producing systems.

Although Bei and Zhang (2007) found that larger-scale, larger-amplitude initial uncertainties generally lead to a larger forecast divergence than did uncertainties of smaller scales and smaller amplitudes, the ten-day simulations of a stable mei-yu period could obtain accurate locations and diurnal variations. However, as moist convection is the key to rapid error growth leading to limited mesoscale predictability (Tan et al., 2004; Bei and Zhang, 2007), the detailed processes of convection, such as MCSs and vortices, obtained by the simulation were not consistent with the observations.

4. Diurnal variation of precipitation and its impact factors

Because the diurnal cyclic lateral boundary conditions were used in the simulation, the diurnal variation was more evident in the simulation than in the observations, which is preferable for analyzing the general diurnal variation and propagation of the precipitation peak from the eastern edge of the TP to the Huaihe River valley during the mei-yu period. As discussed above, the two rainfall maximums were related to the SWV and the MYFV; this section will explain the relationships among the diurnal variation of precipitation, the two MPS circulations, and the two vortices (SWV and MYFV).

4.1. Diurnal variation of precipitation and vortices

Figure 5 shows the wind field, vorticity at 700 hPa and precipitation averaged from the final seven-day simulation

with a three-hour interval. The general characteristics are as follows. The SWV was located near 105°E during the whole day, and the wind-shear line, as well as the vortices related to the MYF, were located to the east of 110°E . Corresponding to the rain belt, the positive vorticity belt extended from the Sichuan Basin to the eastern coastal region with two positive vorticity centers associated with the SWV and the MYFV. The diurnal variation of precipitation showed different diurnal features from the eastern edge of the TP to the east plains. Convection and precipitation over the eastern edge of the TP ($100^{\circ}\text{--}103^{\circ}\text{E}$) gradually developed at 0600 UTC (Fig. 5c) and remained active from the afternoon to the early evening (0600–1800 UTC; Figs. 5c–g). Owing to the cooling of the eastern edge of the TP at night, convection and precipitation tend to weaken during the nighttime. Analyses of the hourly precipitation (not shown) and its anomaly (Fig. 6) illustrate that the rainfall over the Sichuan Basin (105°E) was intensified during the evening and into early the next morning (1000–2100 UTC), with a peak at 1600 UTC, and that the rainfall was suppressed from late morning to the afternoon (0000–0900 UTC), with a minimum value at 0300 UTC. The precipitation along the MYF over the Huaihe River valley peaked from late evening and into early the next morning (1200–0200 UTC; Figs. 5 and 6), representing a delay of approximately two hours compared to the Sichuan Basin rainfall, but maintaining the level for longer (Fig. 6). The weak phase of the MYF precipitation appeared between the morning and early evening (0300–1100 UTC). The simulated diurnal variation of precipitation generally agreed well with the observations (Fig. 4a).

To determine in detail the relationships between the precipitation and vortices over the Sichuan Basin and the MYF, the diurnal variation of the anomalous hourly rain rate and the 850-hPa vorticity averaged for the SWV and MYFV regions (indicated in Fig. 3b) are shown in Fig. 6. The anomalous hourly rain rate is the difference between the hourly rain rate and the daily mean of the final seven-day simulation. It is

noted that the vorticity also showed obvious features of diurnal variation. It is apparent that there were two precipitation peaks in the two vortex regions in one day, the first weak peak being in the afternoon (0600–0900 UTC) and the second one reaching a maximum in the late evening and into the early morning (1600–2000 UTC). However, the first weak peak in the afternoon was much smaller than the maximum nighttime peak, and it was even lower than the daily average rainfall. The peak rainfall associated with the MYFV at 1800 UTC was delayed by approximately two hours compared to that of the Sichuan Basin at 1600 UTC. However, there was only one vorticity peak during 1900–2000 UTC, which occurred 1–2 hours later than the peak rainfall. It seems that the diurnal variation of vorticity was different from that of the rainfall. It is interesting to note that the vorticity decreased to its minimum when the rainfall reached its afternoon peak. In section 5, the vorticity budget equation will be used to analyze the development of the SWV and MYFV and explain why the weak peak of precipitation in the afternoon could not further the development of the vortex.

There are many factors influencing the diurnal variation of precipitation and vorticity, including thermal circulation between land and sea, MPS circulation driven by terrain elevation differences, and local heating. SZ12 showed that the MPS circulation between the second-step terrain and the east plains suppresses convection along the MYF during the daytime and strengthens convection during nighttime. The nocturnal convection intensifies or triggers the MCV, and the eastwardly propagated MCV reinforces the precipitation in the eastern part of the MYF. However, SZ12 ignored the impacts of the TP; the effects of the TP would not only directly influence convection and rainfall over the Sichuan Basin and Chongqing, but also could propagate downstream and influence the triggering and intensity of convective systems along the MYF (Kurosaki and Kimura, 2002; Zhuo et al., 2002; Wang et al., 2004, 2005). Fu et al. (2011) found that there are two primary mechanisms by which convective systems

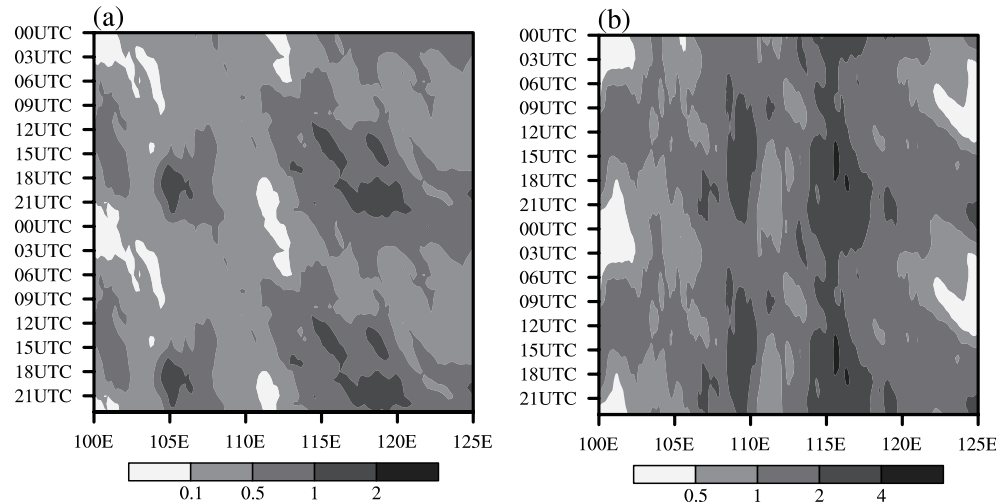


Fig. 4. Time-longitudinal diagram of the rain rate (mm h^{-1}) averaged from the rain belt (Fig. 3) for 4–10 July 2007: (a) CMORPH; (b) Model simulation.

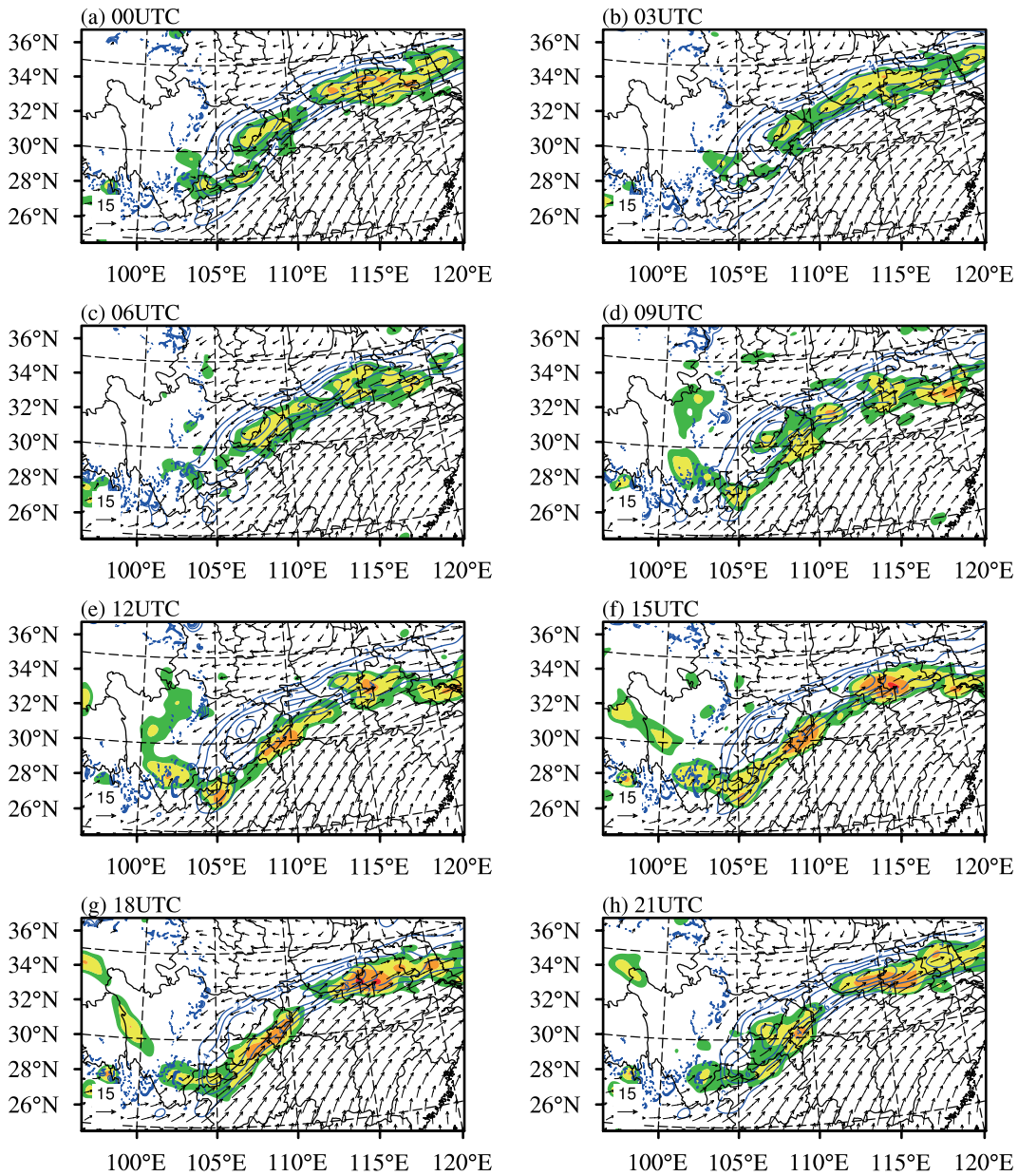


Fig. 5. The simulated diurnal variation of the 700-hPa wind field (arrows), relative vorticity (blue isolines, 10^{-5} s^{-1}) and hourly precipitation (colored areas, mm h^{-1}) averaged from the final seven-day simulation.

influence precipitation along the MYF: (1) The eastwardly propagating convective systems from the eastern edge of the TP trigger the genesis of the SWV or enhance its intensity. The strengthened SWV then enforces the transfer of kinetic energy to the MYF, which would be favorable for the intensification of precipitation at the MYF. (2) An SWV is generated by eastwardly propagating convective systems from the TP, and subsequently moves eastward along the MYF under the leading of a high-level trough, and induces severe heavy rainfall. The second mechanism clearly enhances precipitation at the MYF. However, most SWVs do not move out of the Sichuan Basin, and the second mechanism did not exist in our simulation at all. In addition, the above analysis shows that the strength of the precipitation along the

MYF was delayed relative to that of the SWV, which suggests that the first mechanism may have existed in our simulation. Therefore, under the first influencing mechanism, the semi-idealized simulation was used to analyze the impacts of convection from the eastern edge of the TP on the precipitation of the SWV and the MYFV.

4.2. Diurnal variation of two MPS circulations and their impacts

Simulated daily precipitation averaged from 27°N to 34°N during the final seven-day simulation and topographic elevations are shown in Fig. 7. There was one peak at the eastern edge of the TP and two peaks east of the TP located over the Sichuan Basin and the second-step terrain (108°–

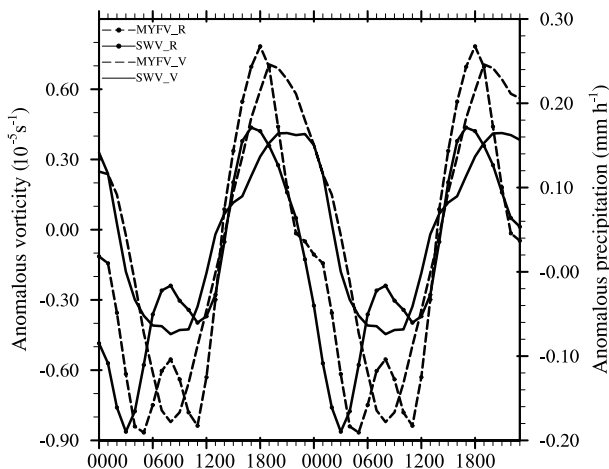


Fig. 6. Diurnal variation of the anomalous hourly rain rate (mm h^{-1}) and 850-hPa vorticity (10^{-5}s^{-1}) averaged for the SWV and MYFV (regions indicated in Fig. 3). The anomalous hourly rain rate is the difference between the hourly rain rate and the daily mean of the final seven-day simulation.

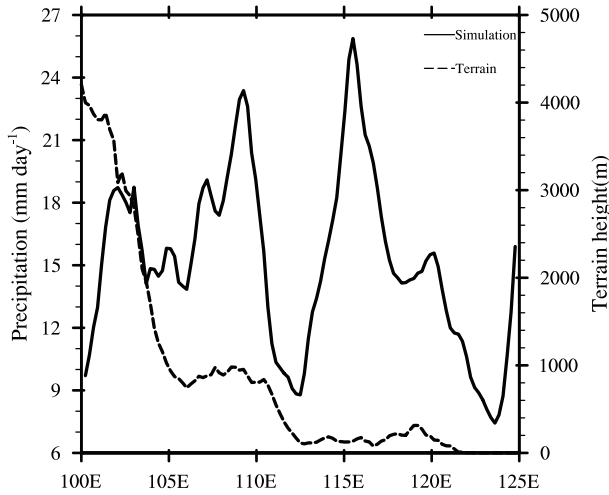


Fig. 7. Map plots of the simulated daily precipitation (solid curve, mm) latitudinally averaged from 27°N to 34°N during the final seven-day simulation. The dashed curve shows the average terrain elevation (m) for 27°N to 34°N .

110°E) and east plains (114°–117°E), with the distance to the highlands being approximately 400–600 km. In the averaged mei-yu period during 2003 to 2007 (Fig. 7a in BZ11), there were only two peaks located at the eastern edge of the TP and over the east plains, but the precipitation peak between the Sichuan Basin and the second-step terrain was not evident. A possible reason is that the SWV always exists in the semi-idealized simulation, which produces much more rainfall than climatological rainfall there. In addition, the two precipitation peaks in Fig. 7 could illustrate the influence of mountains on the enhancement of heavy rainfall, which was discussed in SZ12 through the case study of the impacts of second-step terrain on MYF precipitation.

To clarify diurnal variation of simulated MPS circulations, Fig. 8 showed the perturbation vertical velocity (the perturbation was the hourly velocity anomaly relative to the daily velocity averaged for 24 hours of the final seven-day simulation) and vertical circulation averaged between 27° and 34°N from the eastern edge of the TP to the eastern coastal region, which is similar to Fig. 13 in BZ11. The low temporal and spatial resolutions of the NOAA GFS data, four points per day, used in BZ11 was not enough to recognize the specific features of diurnal MPS circulations in different stages. Moreover, the typical mei-yu only occurred in 2003 and 2007; therefore, in BZ11, average mei-yu circulation from 2003 to 2009 could not show the typical diurnal variation under synoptic mei-yu circulations. Our detailed simulation, however, could be used for analyzing the evolution of two MPS circulations and their impacts on the SWV, the MYFV and the corresponding precipitation during the typical mei-yu period.

At 0600 UTC, due to the differential heating between the TP and Sichuan Basin after sunrise, relative heating on the TP triggered stronger perturbation updraft at the eastern edge of the TP, and the relative cooling in the Sichuan Basin contributed to the generation of perturbation downdraft. Therefore, an MPS circulation (S1) between the eastern edge of the TP and the Sichuan Basin formed and the anomalous ascending motion extended upward and eastward accompanied by strengthened heating at the eastern edge of the TP (Fig. 8c). During the developing stage of S1, there was a weak rainfall peak generated by thermal convection in the afternoon over the Sichuan Basin, which was even weaker than the daily mean precipitation (Fig. 6). In the meantime, due to the heating difference between second-step terrain and the east plains, another MPS circulation (S2) formed. The upward branch and downward branch of S2 started to intensify at 0800 UTC (not shown), and the downward branch of S2 reached its peak at 0900 UTC (Fig. 8d), with the maximum anomalous descending and ascending motions extending to the middle troposphere (approximately 5–10 km). At this point, the MYF precipitation (110°–112°E) reached its weak peak at 0800 UTC (Fig. 6). Some small-scale anomalous rising and descending motions in the S1 circulation during the daytime may have been related to the convective activities of the SWV. Meanwhile, the heating difference between ocean and land contributed to an S3 circulation between the eastern coastal region and its adjacent ocean. At this time, the low-level perturbation easterly wind extended from the eastern coastal region to the foot of the TP and formed up-slope wind.

At 1200 UTC, weak ascending motion shifted to being over the Sichuan Basin (Fig. 8e), followed by the enhancement of precipitation and vorticity (Fig. 6), and a descending motion developed in the upward branch of S2 (Fig. 8e). At 1500 UTC, due to the relatively faster cooling over the TP during nighttime, a descending motion appeared at the eastern edge of the TP, as did an ascending motion in the Sichuan Basin. AS1, the reversal circulation of S1 formed between the Sichuan Basin and the TP (Fig. 8f), which reinforced the

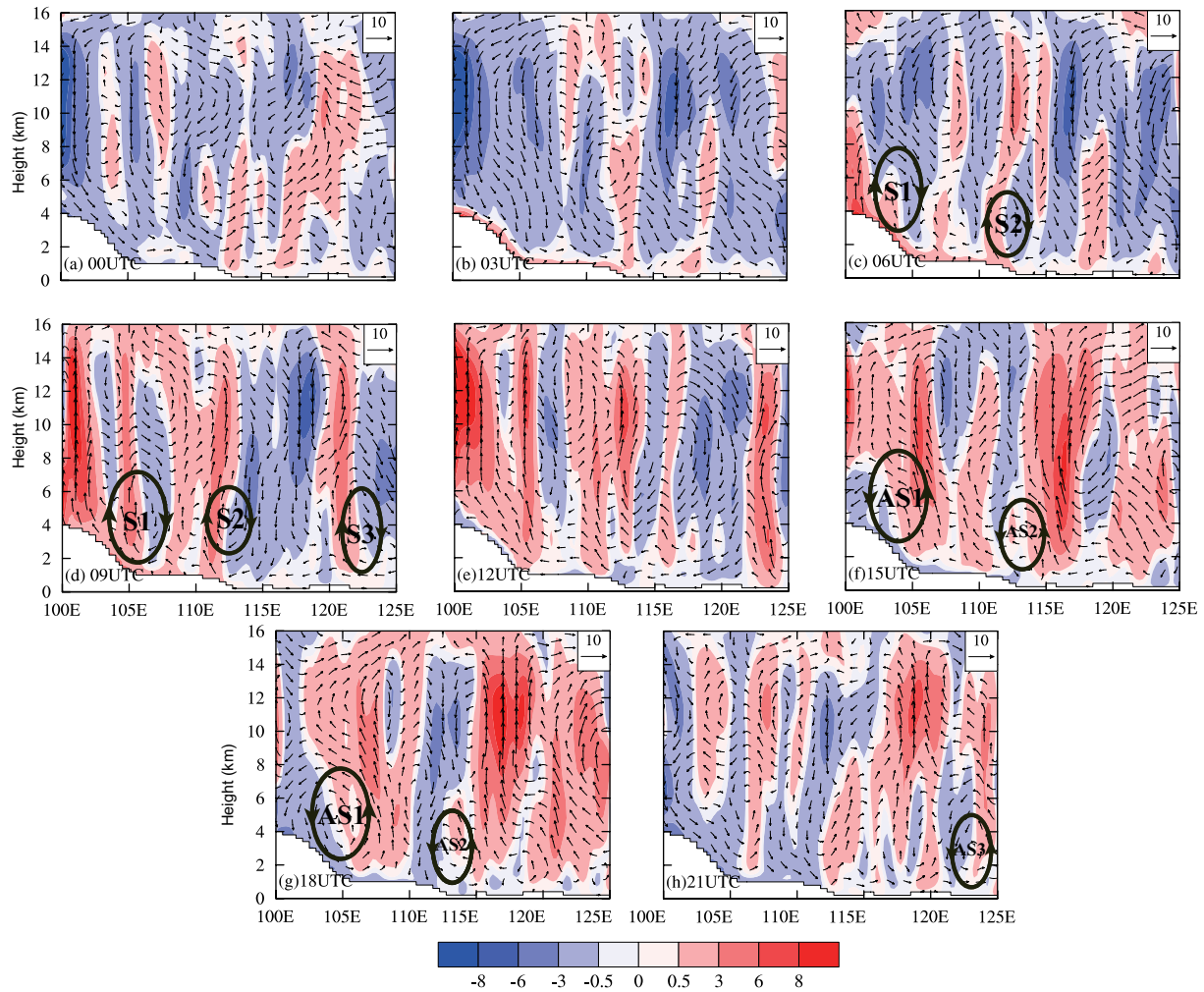


Fig. 8. Height–longitudinal cross section of the diurnal evolution of the perturbation of vertical velocity (colored areas, cm s^{-1}) and vectors of anomalous zonal winds and anomalous vertical velocity ($\times 100$) at three-hour intervals for the final seven-day simulation. The bottom white (unshaded) areas represent the topography, and the black circles indicate the MPS circulations. (a) 0000 UTC, (b) 0300 UTC, (c) 0600 UTC, (d) 0900 UTC, (e) 1200 UTC, (f) 1500 UTC, (g) 1800 UTC and (h) 2100 UTC.

rising motion over the Sichuan Basin and the precipitation of the SWV (Figs. 5 and 6). Meanwhile, daytime S2 circulation converted to nighttime AS2 when the upward branch of S2 over the second-step terrain moved to the Huaihe River valley and its downward branch covered the Taihang-Wushan Mountains. An analysis of an hourly simulation (not shown) revealed that a propagating ascending motion from east of the SWV made a certain contribution to the enhancement of the upward branch of AS2 during the transition period from S2 to AS2 (1200–1500 UTC; Figs. 8e, f). However, the detailed impacts of the SWV on its downstream regions will be discussed in the individual case study in section 5.

AS1 and AS2 circulations developed into their mature stages during the next early morning (1800 UTC), while the two upward branches enhanced precipitation over the Sichuan Basin and the MYF (Fig. 8g), contributing to a diurnal rainfall peak (Figs. 5 and 6). Because the updraft branches of AS1 and AS2 strengthened their local convection and precipitation, vortices in the Sichuan Basin and the

MYF (east of 110°E) had a maximum vorticity of $8 \times 10^{-5} - 10 \times 10^{-5} \text{s}^{-1}$ (Figs. 5f–h and 6). Although the thermal circulation (AS3) between ocean and land was weak at 1800 UTC (Fig. 8g), possibly affected by the effect of convective systems at the MYF, the evident ascending motion over the ocean, as well as the descending motion along the coastline (AS3), could be found at 2100 UTC (Fig. 8h). At the same time, the westerly wind of perturbation below 2 km could be observed from the foothills of the TP to the eastern coastal region. During the morning (0000–0500 UTC; Figs. 8a, b), AS1 and AS2 circulations transited to S1 and S2, except that a weak ascending motion existed over the MYF.

Based on the above discussion, there were three thermal driving circulations in the afternoon and early evening (0600–0900 UTC) from the eastern edge of the TP to the eastern coastal region with the mature stage occurring at 0900 UTC: S1, located between the eastern edge of the TP and Sichuan Basin; S2, developing between the second-step terrain and the east plains; and S3, forced by heating differences between

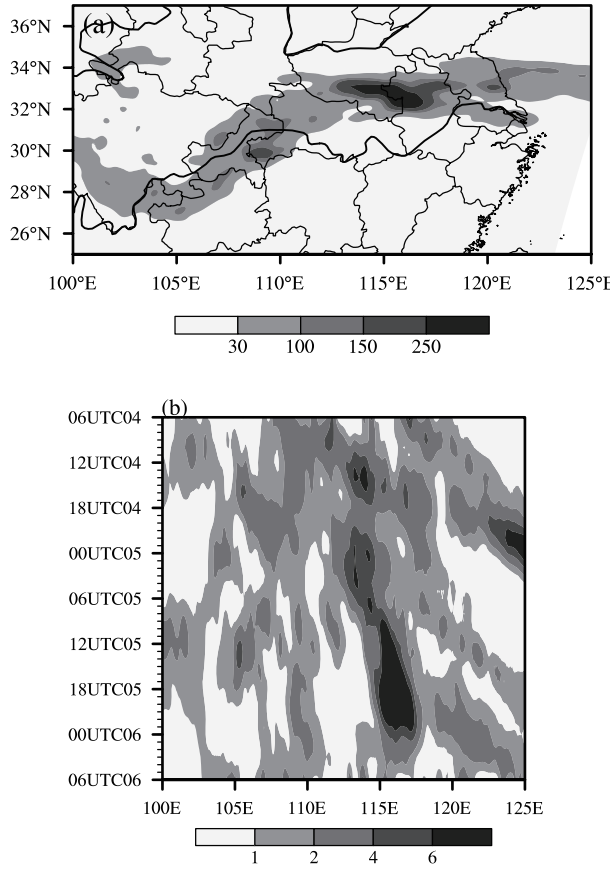


Fig. 9. (a) Simulated accumulated precipitation from 0600 UTC 4 July to 0600 UTC 6 July 2007 (units: mm). (b) Hovmöller time-longitudinal diagram of the simulated rain rate (mm h^{-1}) averaged from the rain belt during 4–6 July 2007.

the land and the surrounding ocean. Downward branches of S1 and S2 circulations suppressed the rising motion in the Sichuan Basin and over the Huaihe River valley and reduced the intensity of precipitation during daytime, with the weak precipitation peak occurring in the afternoon (at approximately 0500–0900 UTC). The transition period of MPS circulations from daytime S1 and S2 to nighttime AS1 and AS2 circulations was in the evening (at approximately 1000–1400 UTC). At midnight and into early the next morning (at approximately 1500–2200 UTC), AS1, AS2 and AS3 circulations, the reversal circulations of S1, S2, S3, formed and matured. Furthermore, the strongest stages of AS1 and AS2 appeared at 1600 UTC (not shown) and 1800 UTC, respectively. Upward branches of AS1 and AS2 enforced rising motion with precipitation peaks in the Sichuan Basin and over the Huaihe River valley. Another transition period of nocturnal circulations to diurnal circulations was from the early morning to noon (approximately 2300–0400 UTC).

Compared to the average MPS circulations during the mei-yu period in BZ11, the heights of S2 and AS2 of the present case in 2007 could have extended to those of S1 and AS1, which means that MPS circulations between the second-step terrain and the east plains became higher than the 5-yr averaged S2 (AS2). There was little difference among

the MPS circulations for warm season precipitation during the pre-mei-yu period (15 May to 15 June), the mei-yu period (15 June to 15 July) and the post-mei-yu period (15 July to 15 August) in BZ11. It is suggested that the average circulation could not represent the typical characteristics of the mei-yu period because there were far fewer days with rainfall than days without rainfall during the period of 15 June to 15 July in 2003–2007.

This section has explained the possible relationship between precipitation from the eastern edge of the TP to the eastern coastal region and two MPS circulations by analyzing average fields of the final seven-day simulation. However, the average field cannot show the continuous evolution of synoptic systems and the relationships among different systems. Moreover, there was a weak precipitation peak in the average diurnal evolution without increased vorticity, which could be explained by individual case analysis. Thus, we chose an individual two-day period during the final seven-day simulation to elucidate the relationships of MPS circulations, vortices and rainfalls, as described in the next section.

5. Individual case analysis

5.1. Case introduction

Three persistent rainfall events consisting of cases on 4–6 July, 6–8 July and 8–10 July, were successfully simulated in our experiment, resembling observed processes well (not shown). According to our reasonable simulation, one of the three heavy rainfall events (from 0600 UTC 4 July to 0600 UTC 6 July) over the Huaihe River valley to the east of the second-step terrain was chosen for a specific case study. The rain belt covered the eastern edge of the TP to the Huaihe River valley with two maxima at 108°–110°E and 114°–117°E (Fig. 9a), which were consistent with the characteristics of the final seven-day simulation in Fig. 3b. It took approximately two days for the rainfall streaks to propagate from the eastern edge of the TP to the eastern coastal region for the average of the final seven-day simulation (Fig. 4b), which is consistent with results in BZ11. The time longitudinal of hourly precipitation shows that the development of rain streaks in the two-day case was similar to the diurnal variation averaged from the final seven-day simulations. Rainfall at the eastern edge of the TP (100°–103°E) began at 0600 UTC and lasted until 1400 UTC. Heavy rainfall over the Sichuan Basin (105°E) occurred in the late evening to early the next morning, which was 2 hours earlier than that along the MYF in the Huaihe River valley. The center of a heavy rainfall maximum appeared over the eastern coastal region (122°E) at approximately 0000 UTC 6 July, and it took approximately 42–45 hours for the rainfall peak to propagate from the eastern edge of the TP to the eastern coastline with a moving speed of 13.5 m s^{-1} , which was similar to the eastward propagating speed of 13 m s^{-1} during the mei-yu period reported in BZ11. Therefore, the simulated case (0600 UTC 4 July to 0600 UTC 6 July) can be considered suitable for further analysis.

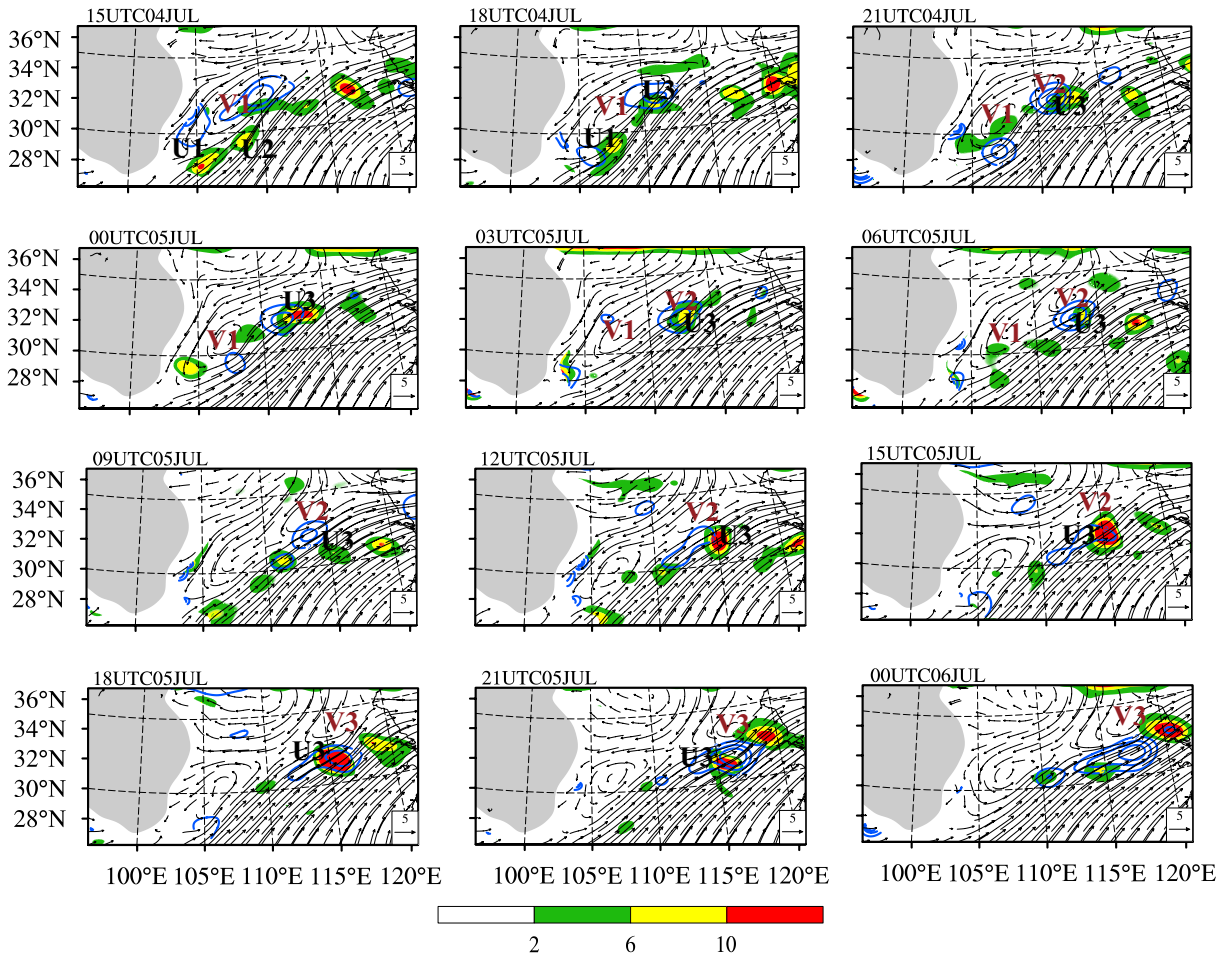


Fig. 10. Simulated 700-hPa horizontal wind (vector, m s^{-1}), anomalous vertical velocity (shaded, cm s^{-1}) and anomalous vorticity (blue solid lines, 10^{-5}s^{-1}) from 1500 UTC 4 July to 0000 UTC 6 July 2007. The anomaly is the hourly difference from the average from 1500 UTC 4 July to 0000 UTC 6 July.

5.2. Impacts of upstream systems on downstream systems

It was shown in BZ11 that the precipitation peak only propagated to 114°E , while SZ12 demonstrated that the nocturnal upward branch of the MPS circulation over the second-step terrain reinforced convection along the MYF and resulted in the generation and propagation of an MCV. The above analysis has clearly shown that a precipitation peak propagating from the eastern edge of the TP to the eastern coastal region is possible. The results of the subsequent activities of rainfall-producing systems from west to east included convection at the eastern edge of the TP in the afternoon, enhanced convection of SWV and MYFV forced by AS1 and AS2 (the upward branches of MPS during the nighttime), and the generation of an eastward moving MCV.

Figure 10 gives wind fields, anomalous vorticity and anomalous vertical velocity at 700 hPa from 1500 UTC 4 July to 0000 UTC 6 July, which was the main development period of the vortices during the entire case. The anomaly is the difference between the hourly data and the data average from 1500 UTC 4 July to 0000 UTC 6 July. There were three vortices at 700 hPa from the Sichuan Basin to the Yangtze River–Huaihe River valley, designated by V1, V2 and V3 in Fig.

10. Figure 11 shows the corresponding height-longitudinal cross section of the diurnal evolution of the perturbations of vertical velocity and vectors of anomalous zonal wind and anomalous vertical velocity at three-hour intervals. The diurnal variations of MPS circulations were less pronounced than the seven-day average fields; however, the continuous evolution of all systems was clear. The quasi-stationary SWV (V1) was intensified during nighttime (1500–2100 UTC 4 July) and became relatively weak during the daytime (0000–0600 UTC 5 July) due to the diurnal variation of MPS (Figs. 10 and 11). V3 (MYFV) occurred on 5 July, which brought heavy rainfall into the Huaihe River valley (Fig. 9), and V2 was a connection between an SWV and an MYFV. Combining the evolution of vortices (Fig. 10) and MPS circulations (Fig. 11), there were three main stages in this individual case: the intensification of SWV (V1) and its convection (Stage 1), the development of V2 (Stage 2), and the triggering of MYFV (V3) and its eastward propagation (Stage 3).

5.2.1. Stage 1: The intensification of SWV (V1)

During 0600–0900 UTC 4 July (not shown), the strong ascending motion developed at the eastern edge of the TP

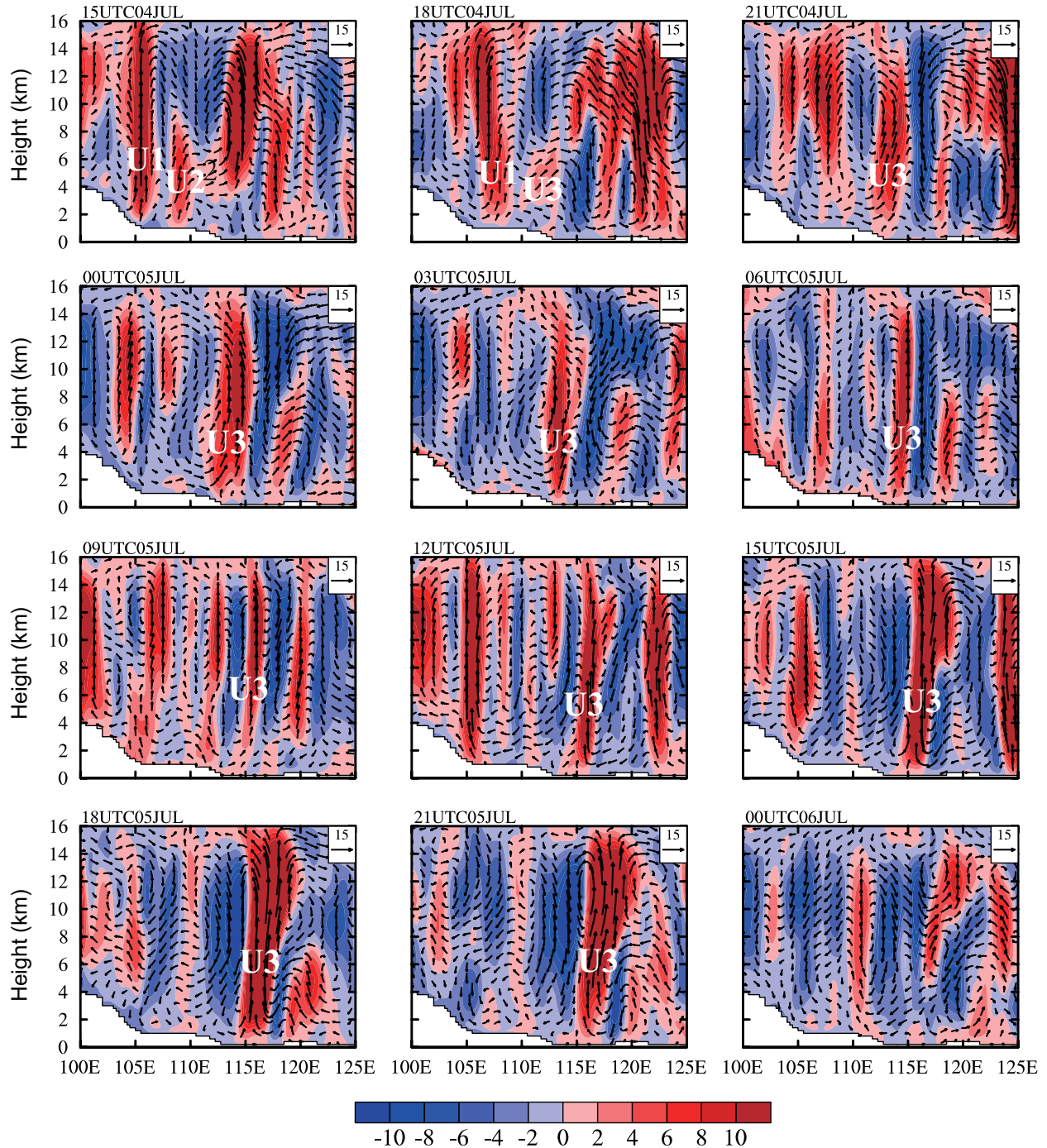


Fig. 11. Height–longitudinal cross section of perturbation vertical velocity (colored, cm s^{-1}) and vectors of anomalous zonal winds and anomalous vertical velocity ($\times 100$) at 3-h intervals from 1500 UTC 4 July to 0000 UTC 6 July 2007. Scales smaller than 300 km are truncated by a Barnes filtering technique (Barnes, 1973; Maddox, 1980). The bottom white (unshaded) areas represent the topography.

and its leeside slope and over the second-step terrain, while the descending motion occurred in the Sichuan Basin and the east plains. Corresponding to the ascending motion over the second-step terrain, a positive anomalous vorticity appeared east of the SWV. At 1500 UTC 4 July, with the development of nocturnal MPS (AS1) (Fig. 11), the upward branch and downward branch of AS1 (taking 104°E as the bound-

ary line) developed in the Sichuan Basin and at the eastern edge of the TP, respectively. Meanwhile, the ascending motion (U2) was triggered to the east of U1 (upward branch of AS1) at 1500 UTC 4 July. The eastward extent of the cyclonic circulation of V1 promoted the low-level convergence and ascending motion at $108^\circ\text{--}110^\circ\text{E}$ (Fig. 10), which was a possible reason for the triggering of U2. When U1 and U2

merged into one upward branch of AS1 at 1800 UTC, an upward branch of nocturnal MPS circulation (AS2) to the east of the second-step terrain was conducive to a new ascending motion (U3) in the middle-low troposphere (at approximately 3–5 km).

5.2.2. Stage 2: The development of V2

At 2100 UTC 4 July, the northeastward-extending V1 (Fig. 10) enhanced the low-level convergence and increased vorticity, causing U3 to develop deeply (Fig. 11). While the upward branch of AS2 over the second-step terrain was mature, U3 and its convection (110°–115°E) were enhanced, which subsequently induced the formation of vortex V2. After the generation of V2, V2/U3 moved eastward to the east plains, enabling the production of heavy rainfall from 2100 UTC 4 July to 0300 UTC 5 July. From 0300 UTC 5 July to 0600 UTC 5 July, the maximum anomalous vorticity and positive perturbation vertical velocity coincided with each other. U3 was weaker because of the suppression of the downdraft branch of S2 during 0600–0900 UTC 4 July. During the daytime, although the downdraft branch of S2 prevented the continuous development of U3, the vorticity of V2 was still in the development trend, which was favorable for convection activities at 113°–115°E. However, the development of V2 during the daytime may have been caused by the topographic effect, as it was located on the leeside of the second-step terrain. During 1200–1500 UTC 5 July, the cyclonic circulation of V2 began to dissipate, but U3 was intensified, forced by the upbranch of AS2.

5.2.3. Stage 3: The triggering of MYFV (V3) and its eastward-propagation

When U3 propagated to approximately 115°E, new convection ahead of V2 triggered a new vortex (V3) at 1800 UTC 5 July (Fig. 10). V3 was an MCV, and the possible formation mechanism has been studied previously (Sun et al., 2010). V3, with closed cyclonic circulation, moved eastward along the MYF from 1800 UTC 5 July to 0000 UTC 6 July. In addition, during maturity, the maximum vorticity of V3 coincided with the positive vertical motion, which also applied for V2/U3. V3 began to decay and the ascending motion transitioned to descending motion after 0000 UTC 6 July because of the transition of the nighttime MPS to the daytime MPS (not shown). During 0300–0600 UTC 6 July, the strong cyclonic wind shear still persisted in the MYF, but the descending motion dominated the MYF with weak precipitation. In addition, observation analyses have revealed a high frequency of MYFV over the east plains (Zhang et al., 2004), and thus the simulated MCV agreed well with the observations.

The above analyses have explained the relationship between two MPS circulations and low-level vortices in the two-day case. Three vortices were identified in this case: V1 was an SWV, while V2 and V3 formed in the middle and lower valley of the Yangtze–Huaihe River valley. V2 and V3 were classified as MYFVs. During the two days, clear diurnal variation of the SWV occurred between 0600 UTC 4 July and 0600 UTC 5 July (Fig. 12), which was similar to the

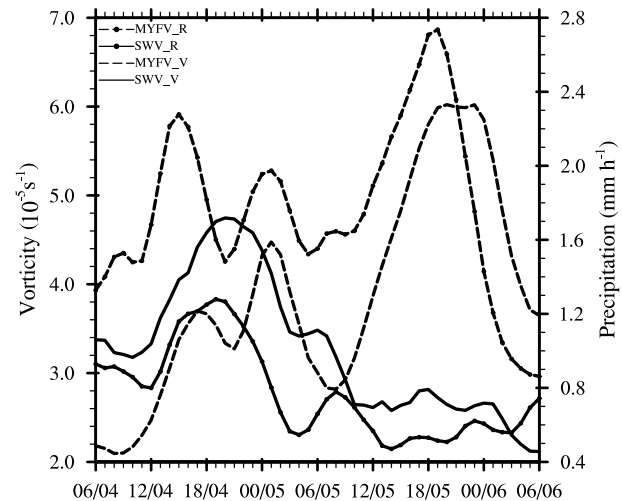


Fig. 12. Evolution of the hourly rain rate (mm h^{-1}) and 850-hPa vorticity (10^{-5}s^{-1}) averaged for the SWV and MYFV from 0600 UTC 4 July to 0600 UTC 6 July 2007 (regions indicated in Fig. 3).

seven-day mean in Fig. 6, with one vorticity peak and two precipitation peaks. The peak precipitation of the SWV in the afternoon (0500–0800 UTC 4 July) also corresponded to low vorticity, as shown in Fig. 6. The vorticity and precipitation of the SWV almost maintained the same intensity without significant diurnal variation from 0600 UTC 5 July to 0600 UTC 6 July. For the vorticity and precipitation of the MYFV, three precipitation peaks (1500–1800 UTC 4 July, 2300 UTC 4 July to 0300 UTC 5 July, and 1600–2100 UTC 5 July) were produced by the upward branches of AS2 and V2 and the composite effects of the upward branch of AS2 and V3. Corresponding to the precipitation peaks, three vorticity peaks also existed, but occurred 1–2 hours later. However, the third peak from midnight of 5 July to the early morning of 6 July was the strongest precipitation peak.

5.3. The vorticity budget of SWV and MYFV

The vorticity budget of SWV and MYFV can be quantified by

$$\begin{aligned} \frac{\partial \zeta}{\partial t} = & -\mathbf{V}_h \cdot \nabla_h(\zeta + f) - \omega \frac{\partial \zeta}{\partial p} + \\ & \text{LHS} \quad \text{HADV} \quad \text{VADV} \\ & \mathbf{k} \cdot \left(\frac{\partial \mathbf{V}_h}{\partial p} \times \nabla_h \omega \right) - (\zeta + f) \nabla_h \cdot \mathbf{V}, \quad (1) \\ & \text{TILT} \quad \text{DIV} \end{aligned}$$

where ζ is the vertical vorticity; $\mathbf{V}_h = u\mathbf{i} + v\mathbf{j}$ is the horizontal velocity vector; $\nabla_h = \frac{\partial}{\partial x}\mathbf{i} + \frac{\partial}{\partial y}\mathbf{j}$ is the horizontal gradient operator; f is the Coriolis parameter; ω is the vertical velocity in the p -coordinate; $\mathbf{i}, \mathbf{j}, \mathbf{k}$ stand for the unit vectors pointing to the east, north and zenith, respectively; HADV and VADV are the terms of the horizontal advection and vertical advection, respectively; TILT stands for tilting, indicating conversion of horizontal vorticity into vertical vorticity

affected by vertical motions; DIV is the abbreviation for divergence, which is the impact of divergence on vortex vorticity; and LHS (left-hand side of the equation) represents the time evolution of vorticity. Friction effects are ignored in the above equation.

Figure 13 showed the vorticity budget of the SWV and MYFV regions at 850 hPa. Although VADV and DIV showed positive contributions, TILT and HADV clearly contributed negatively in the afternoon (0600–0800 UTC 4 July and 0300–1200 UTC 5 July) (Fig. 13a), corresponding to the negative variation of LHS (Fig. 13c). The negative contribution of TILT possibly resulted from the downward branch of MPS

circulation S1, which created little conversion of horizontal vorticity into vertical vorticity. Owing to the upward branch of MPS (AS1) increasing the vertical velocity of the SWV at night (after 10 UTC 4 July), TILT contributed positively to vorticity through the conversion of horizontal vorticity into vertical vorticity. The vorticity budget at 850 hPa of the MYFV showed clear diurnal variation after 0300 UTC 5 July (Figs. 13b, c). In spite of the opposite phases of TILT and VADV, a greater contribution of TILT resulted in decreasing the MYFV vorticity in the afternoon and increasing the MYFV vorticity at night. After 1200 UTC 5 July, other than the positive contribution of TILT, the increased positive contribution of DIV forced the development of the MYFV. However, the DIV of the MYFV made little contribution to this vortex from the evening of 4 July to the early morning of 5 July.

In summary, an upward branch of MPS circulation between the eastern edge of the TP and the Sichuan Basin in the evening enhanced the upward motion and subsequently intensified the precipitation and the SWV (V1). Then, the eastward extent of the cyclonic circulation of the SWV east of 110°E, combined with the upward branch of AS2, triggered vortex V2 in the evening of 4 July. Under this condition, the TILT term contributed more positively to the intensification of the SWV. The negative contribution of TILT weakened the intensity of vortex V2 during the daytime of 5 July because the downdraft branch of S2 suppressed the convection of V2. The eastward propagation of V2 transported horizontal kinetic energy and water vapor into the Huaihe River valley east of 115°E and triggered V3. The positive contributions of TILT and DIV enhanced the development of V3 because of the upward branch of MPS circulation (AS2) in the evening of 5 July. Because vortex V3 was much stronger than V2, the MYF precipitation peaked on the night of 5 July. Although clear diurnal variation of MPS circulation has been demonstrated in previous studies (BZ11; SZ12), the vorticities and precipitations of the SWV and the MYFV had evident nocturnal peaks once in two days, and precipitation peaks of these two vortices were not synchronous.

In addition, to verify the above semi-idealized simulation and results, a sensitivity experiment was considered, similar to that described in section 2 (hereafter referred to as the control run), except that the experiment had a 5-degree westward extending boundary. The results showed that the position and coverage of the rain belt in the sensitivity test were similar to those of the control run with a stronger rainfall maximum (not shown). The verifications of diurnal variations of precipitation and MPS circulation showed that these two experiments produced similar variations, except for the intensity (not shown). The MPS circulations in the sensitivity experiment were somewhat different from those in the control experiment, in which it was indicated that lateral boundary conditions impact upon the activities of individual systems. From those analyses, it appears that the control experiment was not very sensitive to the domain size and that the analyses and results are reasonable.

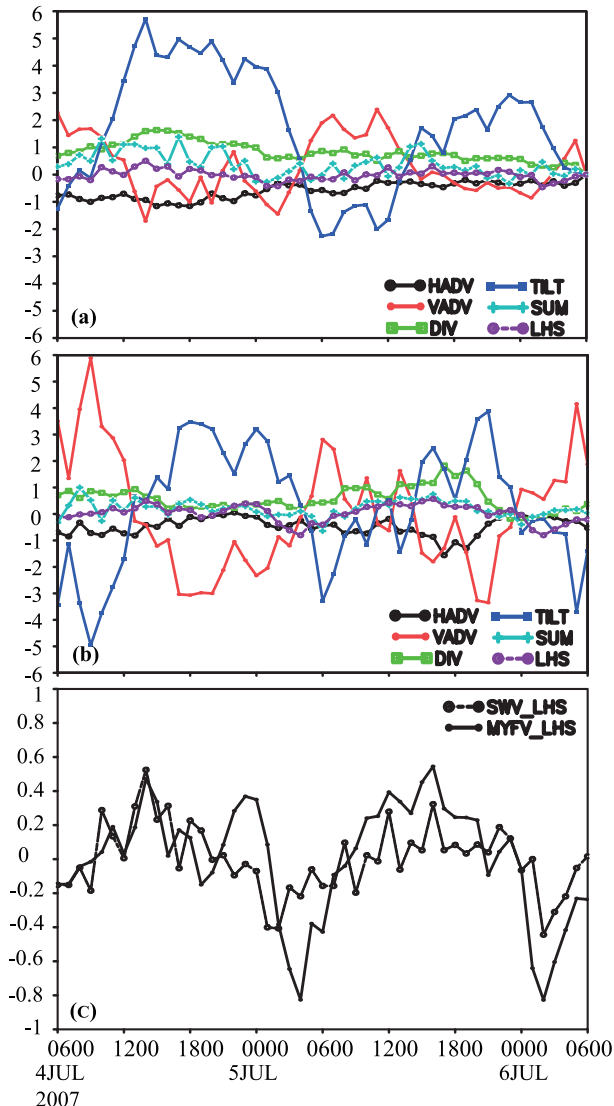


Fig. 13. Terms of the vorticity equation at 850 hPa from 0600 UTC 4 July to 0600 UTC 6 July 2007 (units: 10^{-9} s^{-2}). HADV is horizontal vorticity advection; VADV is vertical vorticity advection; DIV is the term of divergence; and TILT is the tilting term. SUM is the sum of the former four terms, and LHS is the left-hand side of Eq. (1) in the text. (a) Vorticity budget of SWV; (b) vorticity budget of MYFV; (c) left-hand side of Eq. (1) in the text.

6. Concluding remarks

A mesoscale numerical model (WRF) was employed for simulating a mei-yu period (1–10 July 2007) with ten-day average fields at 0000 UTC as the initial field and at 0000 UTC, 0600 UTC, 1200 UTC and 1800 UTC as cyclically lateral boundary fields. Diurnal variations of two MPS circulations associated with specific topographic distributions from the TP to the eastern coastal region (including first-step terrain, the TP, the Sichuan Basin, second-step terrain, and the east plains), and the impacts of these two MPS circulations on the SWV and the MYFV were investigated. To avoid the effect of the average field, an individual case chosen from a simulated event was analyzed in detail to elucidate the complicated relationships among those systems.

Diurnal cyclic initial and lateral boundary conditions were able to simulate the general geographic distribution of precipitation and its diurnal variations from the eastern edge of the TP to the Yangtze River–Huaihe River valleys. The simulation successfully reproduced two precipitation maximum centers related to the SWV and the MYFV in the rain belt, which was consistent with the corresponding observations. The rainfall related to both SWV and MYFV had a weak peak in the afternoon and a strong peak from midnight to the early morning.

Analyses of the averaged final seven-day simulation showed the different diurnal variations of precipitation in different regions. The convection at the eastern edge of the TP was active from the afternoon to the early evening (0600–1800 UTC) due to the accumulated surface diabatic heating during the daytime. The upward branch of MPS circulation (AS1) enhanced the rainfalls in the Sichuan Basin from the early evening to early the next morning (1000–2100 UTC). Subsequently, the eastward movement of the convection/cyclonic shear line of the SWV combined with the upward branch of AS2 resulted in a peak MYF rainfall in the late evening until early the next morning (1200–0200 UTC).

The individual two-day case analysis confirmed that the upward branches of AS1 and AS2 enhanced the precipitation of an SWV and an MYFV. The eastward propagation of rainfall streaks from the mean of the final seven days (Fig. 4b), as well as in the individual case (Fig. 9b), was the result of convective activities of several systems in series from west to east. The eastwardly propagating convective systems from the eastern edge of the TP and the upward branch of MPS (AS1) enhanced the SWV intensity and its convection during the nighttime. Then, the strengthened SWV and its convection extended eastward to trigger an MYFV (V2). Finally, the upward branch of MPS (AS2) enhanced the convection originated from V2 and induced the generation of a stronger MYFV (V3). The strongest vortex (V3) and its eastward propagation produced severe heavy rainfall over the Yangtze River–Huaihe River valleys.

The diurnal variations of precipitation and its influencing factors, and the relationships between MPS circulations and both SWV and MYFV, were analyzed through the semi-idealized simulation using averaged fields as initial and lat-

eral boundary conditions. Some previous studies (Carbone et al., 2002; Carbone and Tuttle, 2008; BZ11) suggest that convection over a plateau or over mountains in the afternoon propagates eastwardly to downstream plains at night-time and enhances the convection/precipitation. However, from the simulations in the present study, it was confirmed that two nocturnal MPS circulations strengthened convection/precipitation at the SWV and MYF regions from the evening to early morning. However, the study did not reveal the specific impact mechanism of the eastward propagation of convection from the TP on the convection/precipitation east of the TP, including areas from the Sichuan Basin and the Yangtze River–Huaihe River valleys to the eastern coastal region. The reason for the lack of a specific mechanism is that it was difficult to distinguish between propagating systems with MYF perturbation because of complex nonlinear effects among a series of mesoscale systems along the MYF and eastward-propagating perturbations. According to the issues discussed above, future work will first focus on the propagation of the TP perturbation and its mechanism using “dry” simulations. If dry convection over the eastern edge of the TP generates the waves/perturbations, and if the drifting waves/perturbations trigger or enhance vertical motion over the downstream plains, we could then add moisture and latent heat to investigate the mechanism and timing of the triggered convection. Furthermore, there only being a peak of the SWV and the MYFV every two days in a mei-yu period, and the potential two-day period, need to be confirmed through both observational data analysis and model simulations in the future.

Acknowledgements. This study was jointly sponsored by a project of the State Key Laboratory of Severe Weather, Chinese Academy of Meteorological Sciences (Grant No. 2011LASW-A15), the National Key Basic Research and Development Project of China (Grant No. 2012CB417201) and the National Natural Science Foundation of China (Grant No. 40930951).

REFERENCES

- Akiyama, T., 1990: Large, synoptic and meso scale variations of Baiu front, during July 1982, Part II: Front structure and disturbances. *J. Meteor. Soc. Japan*, **68**(5), 557–574.
- Bao, X., F. Zhang, and J. Sun, 2011: Diurnal variations of warm-season precipitation east of the Tibetan Plateau over China. *Mon. Wea. Rev.*, **139**(9), 2790–2810.
- Barnes, S. L., 1973: Mesoscale objective analysis using weighted time-series observations. NOAA Technical Memorandum, ERL, NSSL-62, National Severe Storms Laboratory, Norman, OK 73069, 60 pp. [NTIS-COM-73-10781].
- Bei, N., and F. Zhang, 2007: Impacts of initial condition errors on mesoscale predictability of heavy precipitation along the mei-yu front of China. *Quart. J. Roy. Meteor. Soc.*, **133**, 83–99.
- Carbone, R. E., and J. D. Tuttle, 2008: Rainfall occurrence in the United States warm season: The diurnal cycle. *J. Climate*, **21**, 4132–4136.
- Carbone, R. E., J. D. Tuttle, and D. Ahijevych, 2002: Inferences of predictability associated with warm season precipitation

- episodes. *J. Atmos. Sci.*, **59**, 2033–2056.
- Chen, F., and J. Dudhia, 2001: Coupling an advanced land surface–hydrology model with the Penn State–NCAR MM5 modeling system. Part I: Model implementation and sensitivity. *Mon. Wea. Rev.*, **129**, 569–585.
- Ding, Y. H., 1993: *Study on the Lasting Heavy Rainfalls over the Yangtze–Huaihe River Basin in 1991*. China Meteorological Press, Beijing, 255 pp. (in Chinese)
- Dudhia, J., 1989: Numerical study of convection observed during the winter monsoon experiment using a mesoscale two dimensional model. *J. Atmos. Sci.*, **46**, 3077–3107.
- Fu, S. M., J. H. Sun, and S. X. Zhao, 2011: A study of the impacts of the eastward propagation of convective cloud systems over the Tibetan Plateau on the rainfall of Yangtze–Huaihe River basin. *Acta Meteorologica Sinica*, **69**(4), 581–600. (in Chinese)
- Geng, B., and H. Yamada, 2007: Diurnal variations of the meiyu/baiu rain belt. *SOLA*, **3**, 61–64.
- He, H., and F. Zhang, 2010: Diurnal variations of warm-season precipitation over North China. *Mon. Wea. Rev.*, **138**, 1017–1025.
- Hong, S.-Y., and J.-O. J. Lim, 2006: The WRF Single-Moment 6-Class Microphysics Scheme (WSM6). *J. Korean Meteor. Soc.*, **42**, 129–151.
- Hong, S.-Y., J. Dudhia, and S.-H. Chen, 2004: A revised approach to ice microphysical processes for the bulk parameterization of clouds and precipitation. *Mon. Wea. Rev.*, **132**, 103–120.
- Huang, H. L., C. C. Wang, and G. T. J. Chen, 2010: The role of diurnal solenoidal circulation on propagating rainfall episodes near the eastern Tibetan Plateau. *Mon. Wea. Rev.*, **138**, 2975–2989.
- Joyce, R. J., J. E. Janowiak, and P. A. Arkin, 2004: CMORPH: A method that produces global precipitation estimates from passive microwave and infrared data at high spatial and temporal resolution. *J. Hydrometeorology*, **5**, 487–503.
- Kurosaki, Y., and F. Kimura, 2002: Relationship between topography and daytime cloud activity around Tibetan Plateau. *J. Meteor. Soc. Japan*, **80**, 1339–1355.
- Maddox, R. A., 1980: Objective technique for separating macroscale and mesoscale features in meteorological data. *Mon. Wea. Rev.*, **108**, 1108–1121.
- Ninomiya, K., 2000: Large- and meso-a-scale characteristics of Meiyu–Baiu front associated with intense rainfalls in 1–10 July 1991. *J. Meteor. Soc. Japan*, **78**, 141–157.
- Noh, Y., W. G. Cheon, and S. Raasch, 2001: The improvement of the K-profile model for the PBL using LES. Preprints, Presentation at Int. Workshop of Next Generation NWP Models, Seoul, South Korea, Laboratory for Atmospheric Modeling Research, 65–66.
- Skamarock, W. C., J. B. Klemp, and J. Dudhia, 2005: A description of the advanced research WRF version 2. NCAR Tech. Note TN-468+STR, 88 pp.
- Sun, J., and F. Zhang, 2012: Impacts of mountain-plains solenoid on diurnal variations of rainfalls along the mei-yu front over the East China plains. *Mon. Wea. Rev.*, **140**, 379–397.
- Sun, J. H., S. X. Zhao, G. K. Xu, and Q. T. Meng, 2010: Study on a mesoscale convective vortex causing heavy rainfall during the Meiyu season in 2003. *Adv. Atmos. Sci.*, **27**(5), 1193–1209, doi: 10.1007/s00376-009-9156-6.
- Tan, Z., F. Zhang, R. Rotunno, and C. Snyder, 2004: Mesoscale predictability of moist baroclinic waves: experiments with parameterized convection. *J. Atmos. Sci.*, **61**, 1794–1804.
- Tao, S. Y., 1980: *Rainstorm in China*. Science Press, Beijing, 225 pp. (in Chinese)
- Trier, S. B., C. A. Davis, and D. A. Ahijevych, 2006: Mechanisms supporting long-lived episodes of propagating nocturnal convection within a 7-day WRF model simulation. *J. Atmos. Sci.*, **63**, 2437–2461.
- Trier, S. B., C. A. Davis, and D. A. Ahijevych, 2010: Environmental controls on the simulated diurnal cycle of warm-season precipitation in the continental United States. *J. Atmos. Sci.*, **67**, 1066–1090.
- Wang, C. C., G. T. J. Chen, and R. E. Carbone, 2004: A climatology of warm-season cloud patterns over east Asia based on GMS infrared brightness temperature observations. *Mon. Wea. Rev.*, **132**, 1606–1629.
- Wang, C. C., G. T. J. Chen, and R. E. Carbone, 2005: Variability of warm-season cloud episodes over East Asia based on GMS infrared brightness temperature observations. *Mon. Wea. Rev.*, **133**, 1478–1500.
- Yang, W., and D. Yang, 1987: Numerical experiment of the topographic influence of Qinghai-Xizang Plateau in the barotropic atmosphere. *Plateau Meteorology*, **6**(2), 117–128. (in Chinese)
- Yasunari, T., and T. Miwa, 2006: Convective cloud systems over the Tibetan Plateau and their impact on meso-scale disturbance in the meiyu/baiu frontal zone. *J. Meteor. Soc. Japan*, **84**(4), 783–803.
- Ye, D.-Z., and Y.-X. Gao, 1979: *Meteorology of the Tibetan Plateau*. Science Press, Beijing, 122–126. (in Chinese)
- Yu, R. C., T. J. Zhou, and A. Y. Xiong, 2007: Diurnal variations of summer precipitation over contiguous China. *Geophys. Res. Lett.*, **34**, L01704, doi: 10.1029/2006GL028129.
- Zhang, J.-J. and B. Z. Zhu, F. K. Zhu, D. M. Weng, G. W. Sun, J. N. Lu, Y. Q. Peng, and Y. Z. Wang, 1988: *The Advancements of Tibetan Plateau Meteorology*. Science Press, Beijing, 181–183.
- Zhang, S. L., S. Y. Tao, and Q. Y. Zhang, 2002: Large and meso-scale characteristics of intense rainfall in the mid and lower reaches of the Yangtze River. *Chinese Science Bulletin*, **47**(9), 779–786.
- Zhang, X. L., S. Y. Tao, and S. L. Zhang, 2004: Three types of heavy rainstorms associated with mei-yu front. *Chinese J. Atmos. Sci.*, **28**(2), 187–205. (in Chinese)
- Zhao, S. X., S. Y. Tao, and J. H. Sun, 2004: *Study on Mechanism of Formation and Development of Heavy Rainfalls on Mei-yu Front in Yangtze River*. China Meteorological Press, Beijing, 282 pp. (in Chinese)
- Zhao, S. X., L. S. Zhang, and J. H. Sun, 2007: Study of heavy rainfall and related mesoscale systems causing severe flood in Huaihe river basin during the summer of 2007. *Climatic and Environmental Research*, **12**, 713–727. (in Chinese)
- Zhuo, G., X. D. Xu, and L. S. Chen, 2002: Instability of eastward movement and development of convective cloud clusters over Tibetan Plateau. *Journal of Applied Meteorological Science*, **13**(4), 448–456. (in Chinese)